The impact of planetary boundary layer parameterisation over the Yangtze River Delta region, China, part 1: meteorological simulation.

ZHU, A., SHI, L., HUANG, L., GU, Y., WANG, Y., CHAN, A. and LI, L.

2021

The impact of planetary boundary layer parameterisation over the Yangtze River Delta region, China - Part I: meteorological simulation

Ansheng Zhu [a,b], Lishu Shi [a,b], Ling Huang [a,b], Ying Gu [c], Yangjun Wang [a,b], Andy Chan [d], Li Li [a,b*]*

[a] School of Environmental and Chemical Engineering, Shanghai University, Shanghai 200444, China

[b] Key Laboratory of Organic Compound Pollution Control Engineering (MOE), Shanghai University, Shanghai 200444, China

[c] School of air transportation, Shanghai University of Engineering Science, Shanghai 201620, China

[d] Department of Civil Engineering, University of Nottingham Malaysia, Semenyih 43500, Selangor, Malaysia

Correspondence to Li Li (Lily@shu.edu.cn) and Andy Chan (Andy.Chan@nottingham.edu.my)

Abstract: The planetary boundary layer (PBL) is the main region for the exchange of matter, momentum, and energy between land and atmosphere. The transport processes in the PBL determine the distribution of temperature, water vapour, wind speed and other physical quantities and are very important for the simulation of the physical characteristics of the meteorology. Based on the two non-local (YSU, ACM2) and two local closure PBL schemes (MYJ, MYNN) in the Weather Research and Forecasting (WRF) model, seasonal and daily cycles of meteorological variables over the Yangtze River Delta (YRD) region are investigated. It is shown that all four PBL schemes overestimate 10-m wind speed and 2-m temperature, while underestimate relative humidity. Inter-comparisons among the different PBL schemes show that the MYNN scheme results in closer match of 2-m temperature and 10-m wind speed to surface observations in summer, while the MYJ scheme shows the smallest bias of 2-m temperature and relative humidity in winter. Compared to the observed PBL height obtained from a micro-pulse lidar system, the MYNN scheme exhibits lowest mean bias while the ACM2 scheme shows the highest correlation. It is also found that there is a varying degree of sensitivity of the PBL height in winter and summer, respectively; a best-performing PBL scheme should be chosen under different seasons to predict various meteorological conditions over complicated topography like the YRD region.

Keywords: Planetary boundary layer scheme; WRF; seasonal sensitivity; Yangtze River Delta

Highlights

- WRF model performances with four PBL schemes over the YRD region are evaluated.
- Seasonal and diurnal variations of surface meteorological parameters are presented.
- MYNN scheme shows good performance during summer while MYJ scheme performs better in winter.

1 Introduction

Through the interaction of surface forcing and turbulent motion, the planetary boundary layer (PBL) leads to mixed exchange of surface water vapour, heat and upper-level momentum, which in turn affects the near-surface meteorological field and the diffusion of atmospheric pollutants [*Ayotte et al.*, 1996; *Jia and Zhang*, 2020; *Sullivan et al.*, 1994]. The structure and variations of the PBL directly reflect changes in surface thermal conditions and are characterized by significant diurnal variations with temperature. Since the turbulent motion of the PBL is generally much smaller than the horizontal grid spacing of existing small- and medium-scale models, sub-grid scale effects need to be considered [*Bryan et al.*, 2003]. The heat and momentum fluxes in the boundary layer are transported by turbulent motions, which are difficult to resolve on the spatial and temporal scales [*Penchah et al.*, 2017] even with general engineering turbulence models; hence general engineering or application simulations require the introduction of a PBL parameterization scheme to calculate the physical quantities of heat and momentum in the boundary layer [*Draxl et al.*, 2014; *Smith and Thomsen*, 2010].

PBL parameterisation scheme mainly describes the vertical transport of atmospheric momentum, heat, water vapour and other physical quantities in the boundary layer [*Garratt*, 1994]. Uncertainties in the physical parameterisation configurations of models, such as cumulus convection, surface processes, and PBL scheme are some of the main causes of errors in the regional climate modeling system [*Wang et al.*, 2014]. Hence the choice and use of parameterisation schemes is of vital importance for the prediction of meteorological fields within the boundary layer, the trajectory study of air pollutant diffusion and the simulation of large-scale weather systems [*Bright et al.*, 2002; *Han et al.*, 2008; *Li et al.*, 2016, *Oozeer et al.*, 2016]. At present, the parameterisation schemes of numerical models mainly include simple population parameter method, K-profile method, closed method, original asymmetric convection method and spectral diffusion theory [*Hu et al.*, 2010; *Moeng*, 1984; *Shin and Hong*, 2011].

The Weather Research and Forecasting (WRF) [*Skamarock et al.*, 2008], a mesoscale model widely used for weather forecasting and relevant research, provides different boundary layer parameterisation schemes. The spatial resolution of the mesoscale model both in horizontal and vertical directions is finer than that of the large-scale model, therefore the boundary layer process can be resolved with more details with the mesocale model. Given the importance of boundary layer parameterisation scheme to a successful numerical simulation, previous studies have examined the impacts of different PBL schemes on simulated meteorological fields and the applicability of specific schemes at different regions [*Coniglio et al.*, 2013; *Gopalakrishnan et al.*, 2013; *Mohan and Bhati*, 2011; *Smith and Thomsen*, 2010; *Yver et al.*, 2013]. In general, the impact of PBL schemes on simulated meteorology is under the influence of season or time of day, the variables considered and the regional characteristics. Thus, there is no single scheme that outperforms others for different applications.

PBL schemes are used to describe the vertical fluxes of heat, momentum, moisture due to eddy transport within the whole atmospheric column in the turbulent processes [*Banks and Baldasano*, 2016]. The number of unknowns of the equations appearing in a turbulent motion equation set is greater than the number of equations sets, making the original closed equation set non-closed, i.e., a set containing an infinite number of equations is needed to fully describe turbulence. To solve this problem, a finite number of equations is used to approximate the unknown quantity, which is known as turbulence modelling [*Hariprasad et al.*, 2014; *Holt and Raman*, 1988]. One major component of the turbulence processes is whether a local or non-local mixing approach is employed. The local closure schemes obtain the turbulent fluxes using the mean variables and their gradients at each model grid. The non-local closure schemes use multiple vertical levels and profiles of convective boundary layer to determine variables [*Cohen et al.*, 2015]. The sensitivity of different parameterisation schemes is closely related to meteorological and geographical environments. The MM5 model (5^{th} generation Mesoscale model) is used by *Zhang and Zheng* [2004] to simulate surface wind and temperature in the central part of summer in the United States. Results show that the non-local Blackadar (BLK) scheme performs better in predicting the daily cycle of temperature and surface wind speed compared with other schemes. *Sanjay* [2008] shows that the non-local Troen-Mahrt (TM) scheme coupled to the land surface scheme causes boundary layer transition mixing, resulting in low humidity in the boundary layer under the condition of clear air in northwest India. *Kwun et al.* [2009] simulates the ocean surface wind speed during the typhoon using MM5 and WRF in combination with various parameterization schemes. It is found that the wind speed obtained from the WRF coupled with the Yonsei University (YSU) and Mellor-Yamada-Janjić (MYJ) schemes are most consistent with observations. By quantifying the meteorological elements

simulated by four PBL schemes in the WRF model, *Xie et al.* [2012] shows that the PBL height simulated by the MYJ and Bougeault and Lacarrere (BouLac) schemes is higher than that simulated by the YSU and ACM2 schemes. It is more conducive to the upward transport of warm and humid airflow and the development of strong convection. *Ooi et al.* [2018] uses the MYJ scheme and studies the momentum and air pollutant transfers during the monsoon climates of Malaysia. *Hu et al.* [2010] evaluates three PBL schemes in the WRF model and found that the non-local YSU scheme and ACM2 scheme simulated strong daytime boundary layer mixing and entrapment, resulting in higher temperatures and lower humidity, while the local MYJ scheme predicted lower temperature and humidity due to weaker mixing and entrainment. At night the mixing of the YSU scheme is stronger than that of the ACM2 and the MYJ schemes, and the predicted temperature is also higher and humidity was lower. *Wang et al.* [2017a] uses the WRF model coupled with four commonly used PBL schemes to predict the meteorological elements and boundary layer structure in a typical farmland area of China, and finds that the ACM2 scheme shows good performance on both sunny and cloudy days.

Although a number of previous studies have looked at the sensitivity of simulated meteorology to the choice of different parameterisation schemes, their simulation is generally conducted for very short periods (days ~ month) or is usually conducted for a specific meteorological event. Therefore, the conclusions of the studies may not be applicable in other situations. It is also found that in some cases, YSU or ACM2 is reported to be good for day-time calculations while results could be different for night-time period or under a different season. Previous works [*Chu et al.*, 2019; *García-Díez et al.*, 2013; *Kala et al.*, 2015; *Madala et al.*, 2015] have shown that there are seasonal variations of different parameterisation schemes and a single PBL scheme could be inappropriate for annual simulations. Therefore, it is important to consider the seasonal and diurnal variations when choosing the optimal PBL scheme.

The Yangtze River Delta (YRD) is located in the north marine monsoon subtropical climate zone of southeast China, which is one of the fast-developed city clusters in China. In recent years, this region has suffered from serious air pollution [*Li et al.*, 2018; *Li et al.*, 2019a, 2019b], which is generally affected by meteorological conditions and emissions. The topography of the YRD region is very complicated, with mountains in western and southern area, and adjacent to the ocean in eastern region. Besides, the YRD region is located in a transection area between northern and southern region. The weather is generally warm and humid in summer and cool and dry in winter. Thus, the air masses are complex. In this situation, the robust prediction of meteorological conditions will significantly affect the air quality simulation. The objective of this study is hence to investigate the

performance of the turbulence parameterisation scheme in the WRF mesoscale model of boundary laminar flow structure simulations in the YRD region of China. In particular, we focus on the seasonal discrepancy in the study area and assess the respective skill of four different commonly used PBL (YSU, ACM2, MYJ, MYNN) schemes in reproducing the meteorological variables in different seasons and discuss their applicability respectively. Our results could be used for further air quality simulation and air pollution research.

2 Methodology

2.1 WRF configurations

The WRF version 4.0 is a non-hydrostatic mesoscale weather simulation system with flexible resolution and parametric scheme. In this study, three nested domains are configured with horizontal resolution of 36 km, 12 km, and 4 km, respectively (Fig. 1). The coarse D01 (186 × 149) covers most of the East Asia and part of Southeast Asia, while D02 (148 × 241) covers eastern China. D03 (205 × 229) encompasses the entire YRD region. 39 vertical levels with a model top set at 50-hPa are used, the first 19 layers are from the planetary boundary layer. Initial and lateral boundary conditions are based on the 6-hour (1.0°×1.0° resolution) Global Final Analysis (FNL) data, provided by the National Center for Environmental Prediction-National Center for Atmospheric Research (NCEP/NCAR).

The main physical-parameterisation schemes contain the Lin microphysics scheme [*Lin et al.*, 1983], the NOAH land surface scheme [*Chen and Dudhia*, 2001], the Kain–Fritsch (KF) cumulus parameterisation (only used in D01 and D02) [*Kain and Fritsch*, 1993], the Rapid Radiative Transfer Model shortwave radiation scheme and the Rapid Radiative Transfer Model longwave radiation scheme [*Mlawer et al.*, 1997].

Simulations are conducted for July and November 2018, starting at 0000UTC. The whole month is divided into 6 parts. The initial 24 hours are considered as a spin-up period, and the respective outputs during these two periods are excluded from the analysis. The analysis nudging option is switched on above the PBL for the horizontal wind components, potential temperature, and water vapor mixing ratio through three domains.

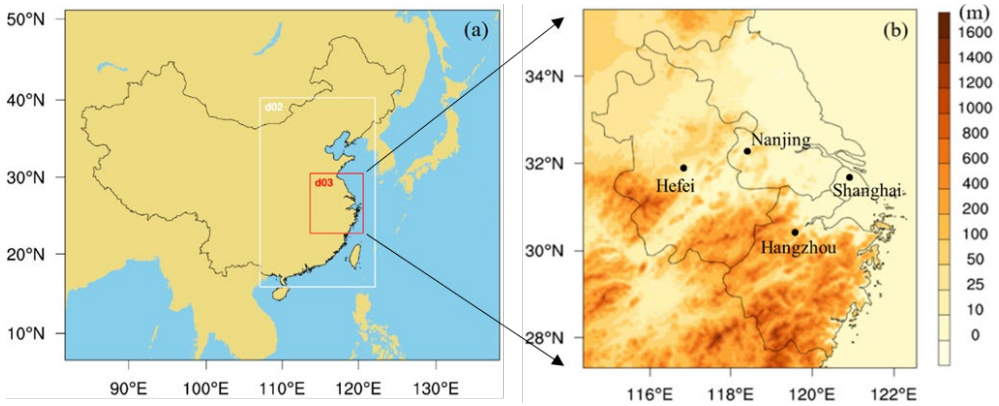

Fig. 1. (a) The three nested modeling domains for WRF model and (b) terrain height for the YRD region

2.2 PBL scheme

Two local closure (MYJ, MYNN) and two non-local (YSU, ACM2) PBL schemes are compared in this study. These four schemes are chosen because they represent the most commonly used schemes in various applications [*Clark et al.*, 2015; *Deppe et al.*, 2013; *Lo et al.*, 2008; *Steele et al.*, 2013; *Su and Fung*, 2015; *Yerramilli et al.*, 2010]. The YSU PBL scheme is a first-order non-local closure scheme. Revised from the Medium-Range Forecast (MRF) scheme, the significant improvement to YSU is the addition of an explicit term for the treatment of entrainment process at the top of YSU. PBL height in the YSU scheme is determined from the Richardson bulk number, with a critical bulk Richardson number of 0.25 over land. This scheme improves the boundary layer diffusion algorithm to allow deeper mixing in windy conditions. Compared to MRF, vertical mixing in the buoyancy driven is increased in YSU scheme and decreased in the mechanic driven situation [*Hong et al.*, 2006]. However, the YSU scheme also shows weakness in mixing with too little over the cold oceans and producing too low nocturnal PBL height [*Hong*, 2010].

The ACM2 scheme [*Pleim, 2007*] is a hybrid first-order scheme, a combination of the ACM1 and local eddy diffusion. It calculates the PBL height above the level of neutral buoyancy when the bulk Richardson number is over 0.25. ACM2 is intended to better represent the shape of the vertical profiles and be more applicable to predict humidity, winds, or trace chemical mixing ratios in the boundary layer scheme. It tends to result in a deeper mixing PBL than other schemes due to its larger critical the bulk Richardson number [*Huang et al.*, 2019].

The MYJ scheme [*Janjić*, 1990] is a one-and-half order local turbulence closure scheme. It diagnoses the vertical mixing process in PBL and free atmosphere through forecasting the TKE, combining with one additional prognostic equation of the TKE. In this method, the upper limit of the main length scale is given, which depends on the turbulence kinetic energy and the shear stress of the buoyancy and driving flow. Under unstable conditions, the equation form of this upper limit

is derived from the turbulent kinetic energy during the growth of turbulence satisfying non-singular conditions. Compared with other schemes, the MYJ scheme shows moister, cooler and little mixing PBL than other schemes since it has a smaller turbulent mixing [*Hu et al.*, 2010].

The MYNN scheme [*Nakanishi and Niino*, 2006] is also a one-and-half order, local closure scheme. To overcome the biases of insufficient growth of convective boundary layer and under-estimated TKE, MYNN considers the effects of buoyancy in the diagnosis of the pressure covariance terms, and uses closure constants in the stability functions and mixing length formulations that are based on large eddy simulation (LES) results rather than observational datasets. This scheme takes into account the effect of buoyancy on the barometric correlation term and introduces the condensation physics process, and is applied to the study of fog events in general [*Chaouch et al.*, 2017; *Li et al.*, 2012; *Román-Cascón et al.*, 2012].

In this study, we conducted WRF simulation with the aforementioned four PBL schemes in four scenarios while the other inputs and parameters keep consistent, so as to look into the impact of different PBL scheme on meteorological simulation in a complicated region like YRD.

2.3 Model performance evaluation

Simulated 2-m surface temperature, 10-m wind speed, relative humidity from four stations at Shanghai (121.336°N 31.198°E), Hangzhou (120.432°N 30.228°E), Nanjing (118.862°N 31.742°E), Hefei (117.298°N 31.780°E) are compared with the hourly meteorological observations for model performance evaluation. The observational data are obtained from the National Oceanic and Atmospheric Administration (NOAA)'s National Climate Data Center archive (http://www.ncdc.noaa.gov/oa/ncdc.html). Meteorology variables are evaluated in terms of mean bias (MB), root of mean square error (RMSE), and correlation coefficient (R):

$$\mathrm{MB} = \frac{1}{N}\sum_{i=1}^{N}(M_i - O_i) \quad (1)$$

$$\mathrm{RMSE} = \sqrt{\frac{1}{N}\sum_{i=1}^{N}(M_i - O_i)^2} \quad (2)$$

$$\mathrm{R} = \frac{1}{N}\sum_{i=1}^{N}\frac{(M_i-\bar{M})(O_i-\bar{O})}{\sqrt{\frac{1}{N}\sum_{i=1}^{N}(M_i-\bar{M})^2}\sqrt{\frac{1}{N}\sum_{i=1}^{N}(O_i-\bar{O})^2}} \quad (3)$$

where M and O refer to the simulated and observed meteorological values, respectively. N represents the number of data pairs.

3 Results and discussions

3.1 Comparison of surface meteorological variables

Tables 1 and 2 show the MB, RMSE and R between the WRF simulated meteorological factors and the observations at four meteorological stations. Figures 2, 4 and 6 show the time series of predicted and observed meteorology variables.

3.1.1 2-m temperature

The temporal series of the WRF model-simulated meteorological variables against observations from the four stations of July is shown in Fig. 2a. All four PBL schemes provide certain overestimations at the beginning of July, however, the simulated 2-m temperatures are generally consistent with the observed values, which is common for temperature simulations [*Giannaros et al.*, 2013; *Hogrefe et al.*, 2015; *Mallard et al.*, 2014; *Mughal et al.*, 2019; *Wang et al.*, 2017b]. In terms of individual cases during the summer, all the four PBL schemes perform well in the prediction of 2-m temperature in Shanghai, Nanjing and Hangzhou, while all the four PBL schemes overestimate 2-m temperature in Hefei. The YSU and ACM2 schemes perform better than the MYJ and MYNN schemes at 2-m temperature with least MB (0.02℃) of YSU and highest R (0.77) of ACM2 (Table 1). *Shin and Hong* [2011] also reports positive biases with the different PBL schemes. In terms of RMSE and correlation coefficient in summer, ACM2 scheme is also better than other schemes. It is reasonable to infer that the overestimation of simulated 2-m temperature of four PBL schemes at Hefei is in large part due to a notable overestimation in the early and mid-July. Among which the MYNN scheme provides the highest correlation coefficient. In general, the average observed temperature in summer is 29.82℃ and the average of YSU scheme is closest to the observation with 29.87℃. The discrepancies of the short-wave radiation reaching the ground simulated by each PBL scheme and its own treatment of turbulence mixing can result in different temperature simulations by different PBL schemes.

Different from summer, simulations of 2-m temperature are overestimated at all sites in winter (Fig. 2b). The main reason is that the boundary layer is mostly in a steady stable state in winter, and coupled with the influence of complex topography, strong inversion temperature, insufficient development of turbulence in the near-surface layer, and the transport of material and energy is dominated by the local area. The MYNN scheme overestimates the most among all cases. In Shanghai, the YSU scheme shows the lowest MB of 0.83℃, the ACM2 and MYJ schemes perform slightly better with high correlation coefficient of 0.87 (Table 2). Though the simulations of the YSU, ACM2 and MYJ schemes are close, 2-m temperature simulations of local closure MYJ scheme are better than those of non-local closure YSU and ACM2 schemes. Simulated 2-m

temperature deviates from observation more in winter than that in summer while the consistency of winter is much better than summer on the whole. This is probably due to the lower temperature in winter and the smaller amplitude variation brought about by the simulation compared to summer.

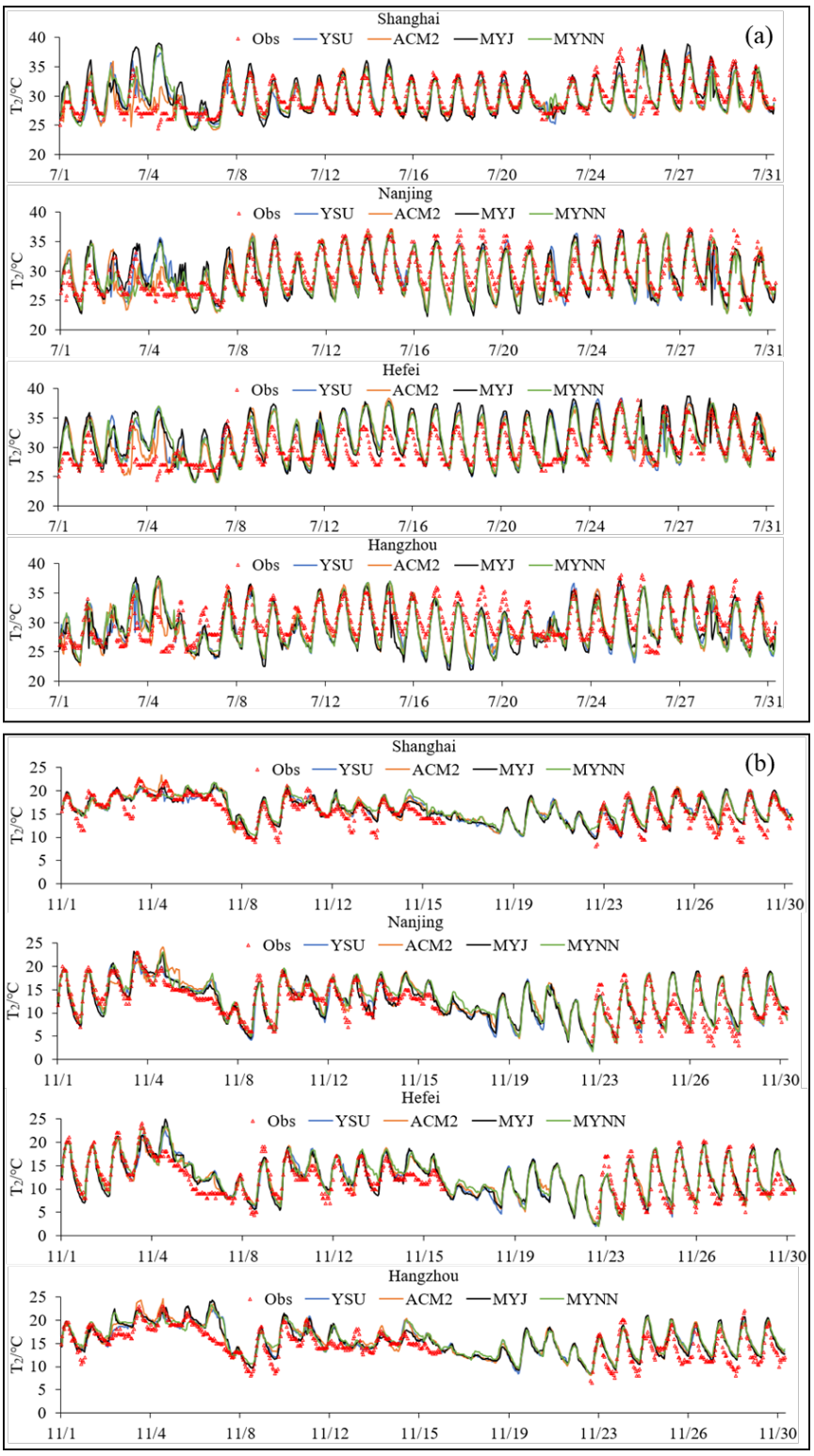

Fig. 2. Time series of 2-m temperature predicted with WRF against observations at four sites for summer (a) and winter (b).

Comparing the average diurnal changes of 2-m temperature, it can be seen that all four PBL schemes

could reflect the diurnal variations reasonably well (Fig. 3a, 3b). Due to the different treatment of physical processes in the boundary layer, even if the same land surface parameters are used, the difference in surface turbulence transportation will cause significant discrepancies in the simulated surface temperature of the four experiments [*Lee et al.*, 2006]. In summer, the daytime simulations of 2-m temperature are generally higher than the observations, but lower than observations at night (Fig. 3c). On the contrary, during winter night, the simulations exhibit overestimation (Fig. 3d). *Hariprasad et al.* [2014] also find that most PBL schemes produce a warm bias in the daytime air temperature and a slight cold bias in the night time air temperature in India. The main reason for the overestimation in summer daytime is that the YRD region is located in the intersection zone of land and sea. Under the influence of the summer monsoon, the water vapor transport is stronger in the daytime. A small cold bias is observed during the summer night which may be attributed to an overestimation of the surface cooling rate during the PBL collapse. Similar finding is also reported by *Cuchiara et al.* [2014]. The MYNN performs the least overestimation in summer daytime with 0.12℃. YSU and ACM2 schemes produce higher temperatures than MYJ and MYNN schemes during the summer nighttime due to its enhanced vertical mixing in the lower PBL [*Hu et al.*, 2010]. The differences in the 2-m temperature simulations of the four PBL schemes at night (Fig. 3c 3d) indicating that there are differences in the four PBL schemes treatment of the stable stratification at night. The surface temperature simulated by the local closure MYJ scheme during winter night is better than that simulated by the non-local closure schemes. The boundary layer is in a steady state during winter, especially due to the influence of valley topography with strong inversion temperature, near-surface turbulence is not fully developed, material and energy transport are mainly local.

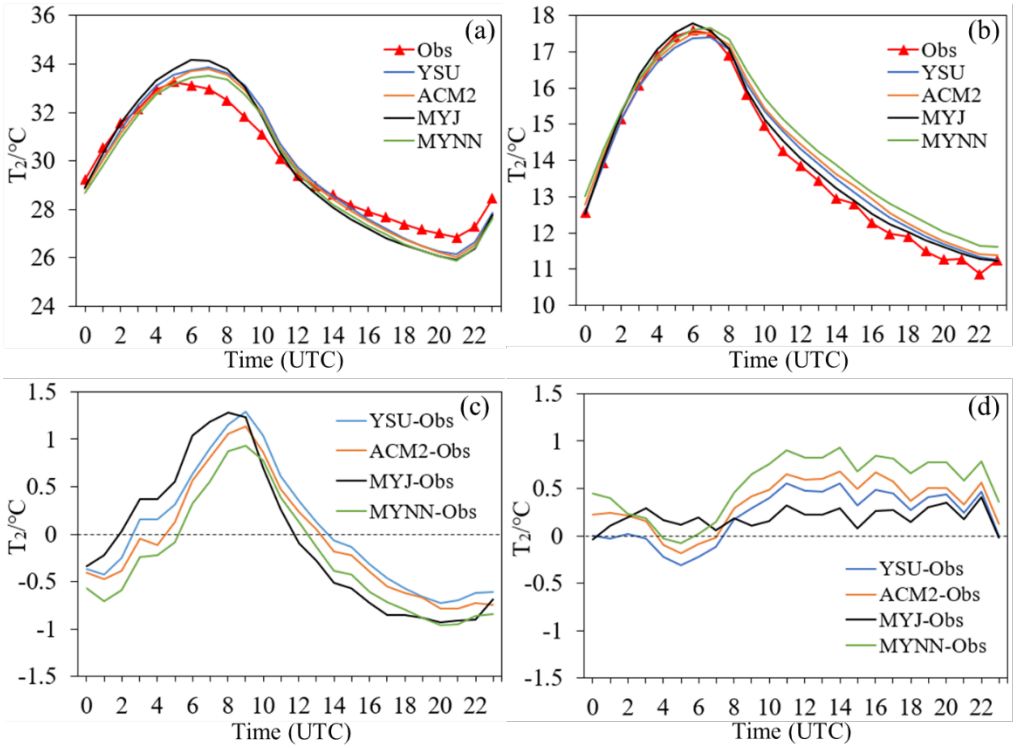

Fig. 3. Average diurnal changes of 2-m temperature for summer (a) and winter (b); Average diurnal differences of 2-m temperature for summer (c) and winter (d)

3.1.2 10-m wind speed

All four PBL schemes overestimate 10 m-wind speed over the YRD region in (Fig. 4), however, there are some differences among the cities due to their specific locations. Different from Shanghai, located along the coastline, the other three sites are all located in inner YRD region, closer to the western or southern hills. The WRF model is unable to capture this special geographical environment as well as sub-grid scale local fluctuations, resulting in the overestimations. *Jiménez et al.* [2012] also reports that wind speed was overestimated in the plains and valleys. The ACM2, MYNN and YSU schemes underestimate 10 m-wind speed in Shanghai in summer, while the MYJ scheme shows overestimation. All the four schemes exhibit overestimation in the other three cities. Among them, the MYNN scheme is the least underestimated with the lowest MB of 0.31 m s^{-1} in summer (Table 1) while the MYJ scheme shows the highest correlation coefficient of 0.59 (Table 2). Other studies have also shown a general tendency of overestimation regarding the 10-m wind speed simulation [*Cheng et al.*, 2005; *Mölders*, 2008]. The discrepancies in wind speed simulation from the different schemes may be caused by different mixing lengths due to various turbulence coefficients and friction velocities for each scheme.

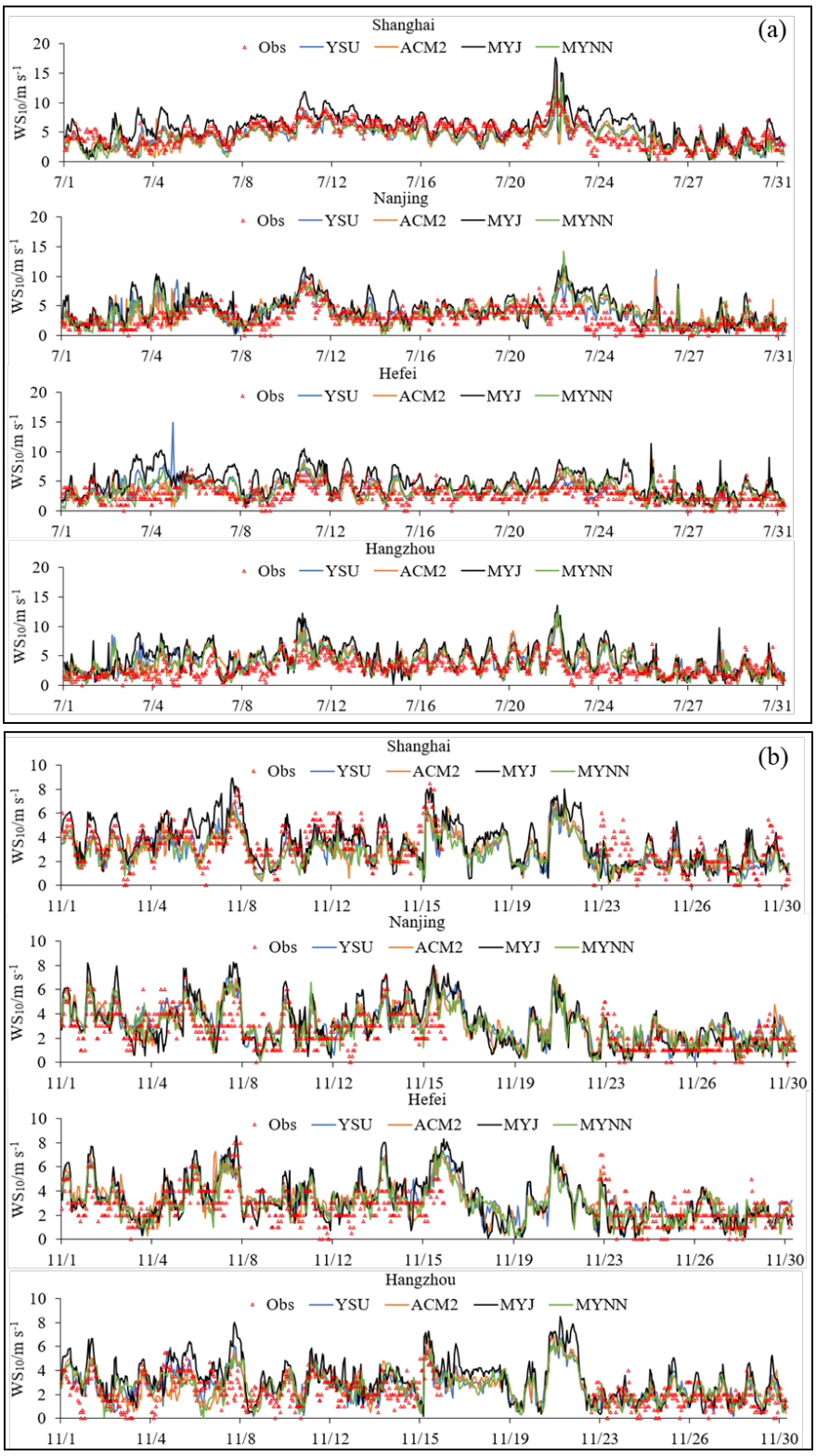

306

307 Fig. 4. Time series of 10-m wind speed predicted with WRF against observations at four sites for summer (a) and

308 winter (b).

309 Similar to July, all four PBL schemes overestimate 10 m-wind speed in Nanjing, Hangzhou and

310 Hefei in November, but the gap becomes narrower. Relative to the lower consistency of Hefei

311 simulations in summer, the overall consistency of the winter simulations is better, with all

correlation coefficient higher than 0.54. Wind speed fluctuates more in summer than in winter, both in observations and simulations. Among the four PBL schemes, the MYJ scheme produces the most obvious level of fluctuations. The 10-m wind speed simulations in winter are much closer to observations than summer, and all four PBL schemes perform much better compared to the summer simulations. Seasonal diurnal variation also corresponds to the good performance of ACM2 and MYNN (Fig. 5). Simulations in winter are close to the observations before 0800UTC, and higher than observations after 0800UTC (Fig. 5b). The reason is partly due to the overestimation of the surface friction velocity at night. The MYNN scheme provides the lowest bias throughout the day in summer as well as night hours in winter (Fig. 5c 5d). This is expected since the MYNN is based on local closure, which is better suited for stable conditions prevailing in winter. This is also possibly due to higher diffusivity coefficients simulated by ACM2 and MYNN [*Hariprasad et al.*, 2014], which exhibit lower wind speed and subsequent less errors compared with other schemes.

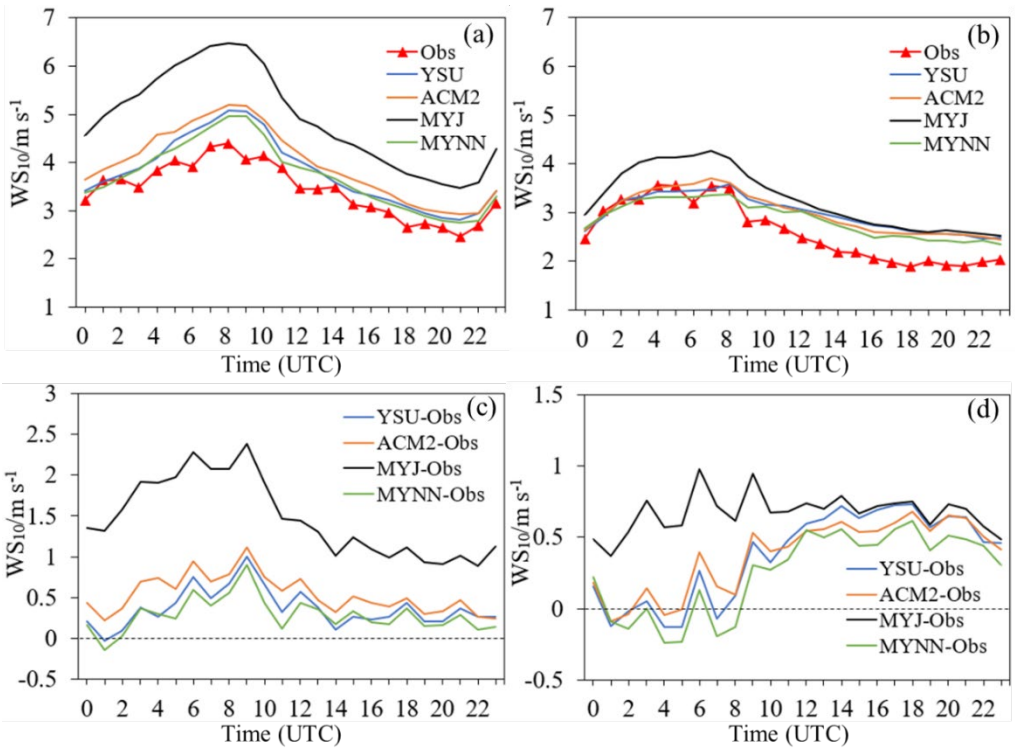

Fig. 5. Average diurnal changes of 10-m wind speed for summer (a) and winter (b); Average diurnal differences of 10-m wind speed for summer (c) and winter (d)

3.1.3 Relative humidity

As for relative humidity, all four PBL schemes mostly exhibit underestimations. Underestimation of humidity by MYJ and YSU schemes is also reported by *Misenis and Zhang* [2010] in air quality simulations over the coastal Mississippi. It can be seen from Table 1 and 2 that MYNN scheme shows the lowest RMSE of 12.74 and highest correlation coefficient of 0.67 in summer (Fig. 6a), MYJ scheme provides the lowest MB of -5.86 and relatively good correlation coefficient of 0.69 in

winter (Fig. 6b). The underestimation of humidity is greater in winter than that in summer. This may be attributed to the moisture content of the atmosphere, which is inherently small in winter, and the diurnal temperature variation becomes the dominant factor in relative humidity changes.

In winter, due to weak mixing and clamping, the relative humidity simulation of MYJ scheme is higher than the other schemes. The non-local scheme ACM2 produced a large dry bias in both summer and winter. Overall MYNN and MYJ simulated the surface relative humidity reasonably well in summer and winter, respectively. The above results are similar to those found in *García-Díez et al.* [2013] over Europe.

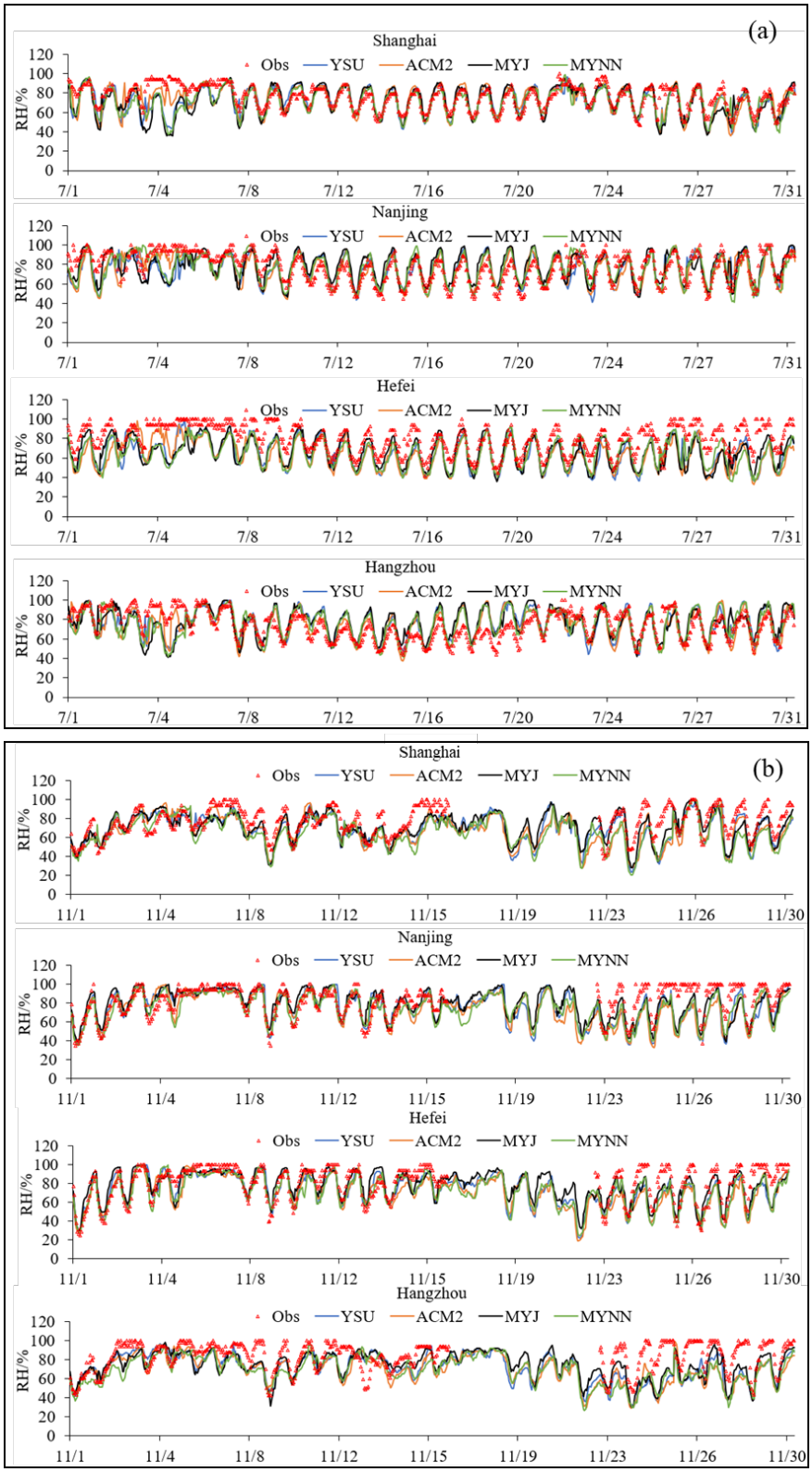

Fig. 6. Time series of relative humidity predicted with WRF against observations at four sites for summer (a) and winter (b).

The diurnal variation of relative humidity is relatively well reproduced with all PBL schemes. Relative humidity is not an output of the model but inferred from temperature, water vapor mixing ratio, and surface pressure. All four PBL schemes show different degrees of underestimations.

During daytime in summer, strong underestimation is shown with all PBL schemes and dry bias becomes smaller at night hours (Fig. 7a). It is shown that MYJ simulates the relative humidity better. In winter, all PBL schemes provide dry bias during day and night hours (Fig. 7b). *Gunwani and Mohan* [2017] also reports that in temperate zone higher dry bias is predicted by all PBL schemes compared to other climate zones. The boundary layer simulated by the non-local YSU and ACM2 schemes has the characteristics of strong mixing and strong coiling, resulting in higher temperature and lower relative humidity simulations. While due to the weak mixing and clamping of local MYJ scheme, the relative humidity simulation is high compared to other three PBL schemes (Fig. 7c 7d). Consistent with a slight warm bias produced by the ACM2 in the northern area of the YRD region, wet bias simulation is found in the same area during summer (Fig. S3). The MYJ scheme exhibits lower simulation of relative humidity than other three schemes in summer while produces obvious higher simulation in winter (Fig. S3).

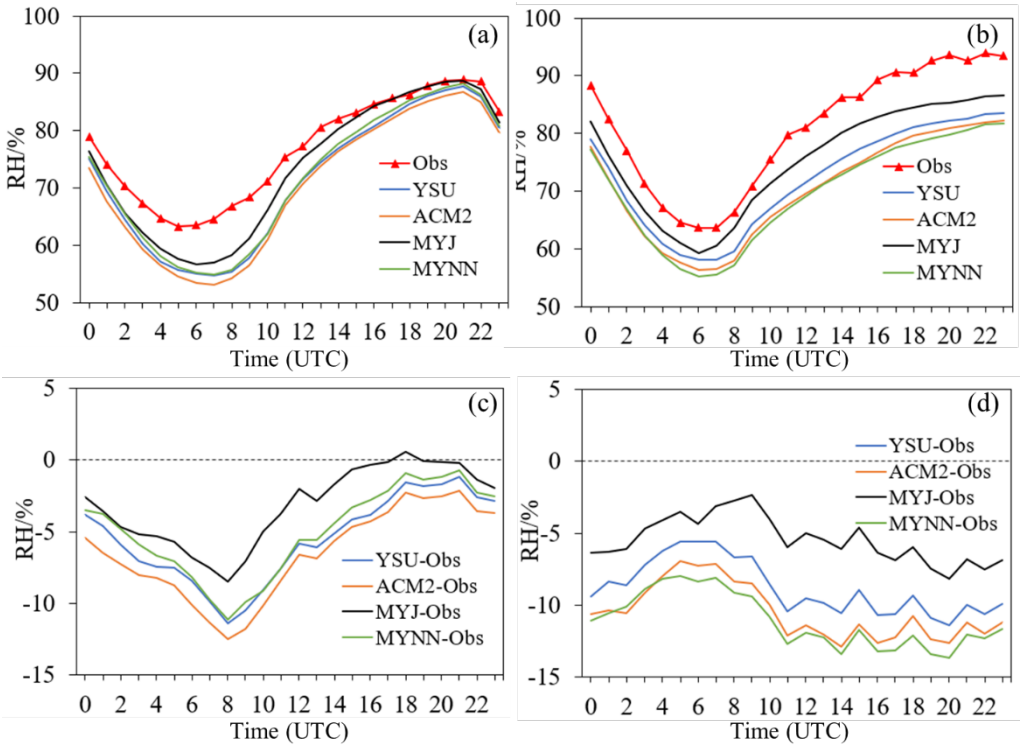

Fig. 7. Average diurnal changes of relative humidity for summer (a) and winter (b); Average diurnal differences of relative humidity for summer (c) and winter (d)

3.2 Comparison of PBL height

3.2.1 Temporal variations of PBL height

One of the largest sources of biases in mesoscale model simulations is the diagnosis of the PBL height. Estimates of the hourly PBL height between 0800 and 1700LST during July are determined based on observations from a micropulse lidar (MPL) at Hefei Environmental Protection Bureau

(31.78 N, 117.20 E) and the PBL height corresponding to the same time in hour during November are calculated at Dianshanhu in Shanghai (31.09 N, 120.98 E). Due to the instrument limitations, the PBL height at night and early morning is not available. Based on the available hourly PBL data, the WRF model simulations are compared.

Fig. 8 compares the hourly observed PBL height with those simulated by the WRF model. The ACM2 scheme leads to the highest overestimation with MB of 0.19 km. The MYNN scheme exhibits the lowest MB of 0.04 km. Time-series comparisons for July of four PBL schemes simulations to the lidar measurement is provided in Fig. 8b. The strong diurnal daytime PBL patterns are captured in all four experiments especially for the MYNN and YSU schemes; however, four schemes exhibit varying degrees of overestimations at daytime-maximum PBL height. The YSU scheme exhibits the highest underestimation with MB of -0.22 km while the MYNN shows the lowest discrepancies compared to the MPL estimate with a difference of -0.04 km. The ACM2 scheme shows the best performance in which the correlation coefficient was 0.92 and the MYNN scheme demonstrates relatively a good result of 0.91. Comparison of PBL height in the daytime during winter is shown in Fig. 8c. From 1100LST to 1500LST all PBL schemes overestimates the PBL height. The MYNN scheme produces the highest overestimation while the MYJ and YSU schemes exhibit closer simulation. The MYJ scheme produces the lowest MB of -0.02km while the MYNN exhibits the highest correlation coefficient of 0.63. Month-series comparisons for November is not so good as July. During 6-8 and 27-30 of November, most PBL schemes show overestimation in the daytime (Fig. 8d).

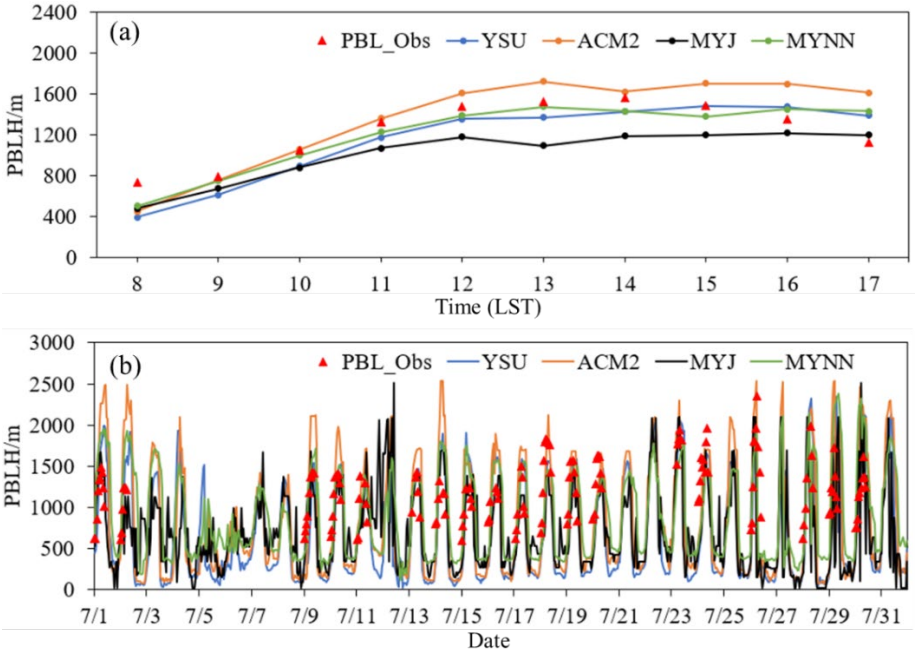

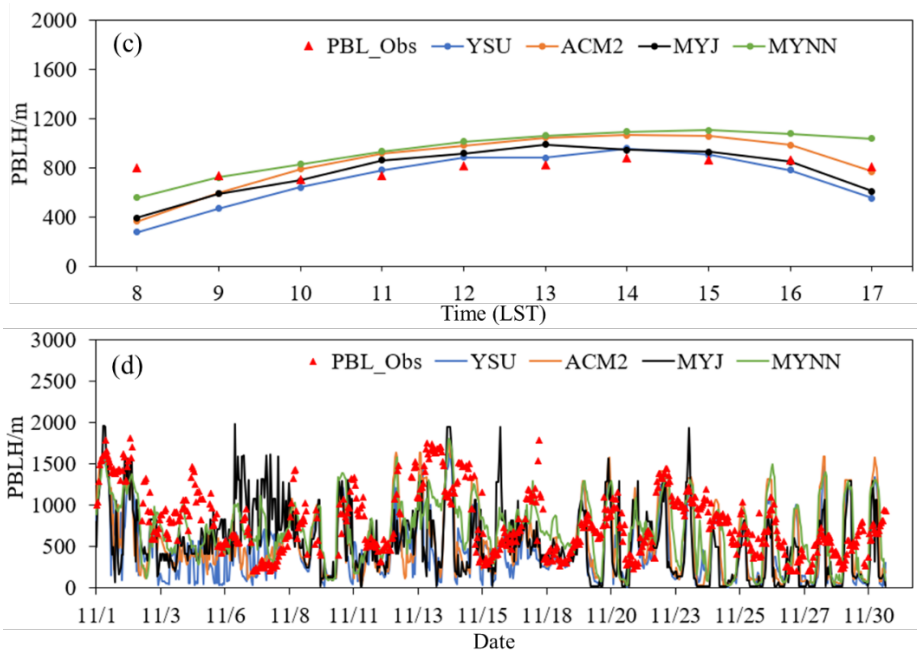

Fig. 8. (a) Time series of daytime PBL heights simulations and hourly average from the lidar in July 2018. (b) Time series of monthly PBL heights simulated by WRF and available hourly average from the lidar of July 2018. (c) Time series of daytime PBL heights simulations and hourly average from the lidar in November 2018. (b) Time series of monthly PBL heights simulated by WRF and available hourly average from the lidar of November 2018.

3.2.2 Spatial distribution of PBL height

Spatial discrepancies of PBL height between the four PBL schemes are evident during different seasons (Fig. S4). PBL height in the inland area of the YRD region during summer is significantly higher than that in winter. In summer, the temperature stratification of the surface atmosphere is unstable, turbulence and turbulent exchange will increase accordingly [*Zhang et al.*, 2011]. Therefore, compared with winter, the more intense convection and turbulence in the summer provides favorable dynamic conditions for the development of the deep boundary layer. While the PBL height is higher in winter than in summer along the coastal area. Due to the differences in the thermal properties of the sea route, the southeast wind prevails in summer and the northwest wind prevails in winter over the YRD region [*Ni et al.*, 2018; *Shen et al.*, 2019; *Li et al.*, 2021]. In summer, the prevailing southeast wind transports the warm and humid airflow to the relatively colder sea surface, which makes it easier to form a stable boundary layer, thus reducing the PBL height; while in winter, the strong northwest wind transports a large number of cold air masses to the warm sea surface, increasing the sensible and latent heat fluxes upward at the sea-air interface, causing the instability of the lower boundary layer and resulting in an increase in the PBL height.

411 Table 1 Statistics of WRF model performance with different PBL schemes in July, 2018

	Shanghai			Nanjing			Hangzhou			Hefei			Average		
	MB	RMSE	R	MB	RMSE	R	MB	RMSE	R	MB	RMSE	R	MB	RMSE	R
								T_2/℃							
YSU	-0.31	2.00	0.74	-0.34	2.12	0.82	-0.89	2.62	0.73	1.62	2.84	0.76	0.02	2.42	0.73
ACM2	-0.49	1.72	0.83	-0.41	1.97	0.85	-1.03	2.26	0.82	1.65	2.88	0.76	-0.07	2.25	0.77
MYJ	-0.13	1.85	0.81	-0.69	2.23	0.82	-1.03	2.69	0.73	1.61	2.92	0.76	-0.06	2.46	0.74
MYNN	-0.41	1.93	0.76	-0.69	1.95	0.86	-1.17	2.54	0.77	1.32	2.56	0.78	-0.24	2.27	0.76
								WS_{10}/ms^{-1}							
YSU	-0.48	1.53	0.70	0.72	1.82	0.55	1.02	1.98	0.50	0.29	1.59	0.41	0.39	1.74	0.55
ACM2	-0.35	1.50	0.70	0.97	1.97	0.56	1.30	2.21	0.49	0.32	1.60	0.42	0.56	1.84	0.54
MYJ	1.19	2.21	0.63	1.33	2.51	0.49	1.62	2.60	0.52	1.68	2.64	0.32	1.46	2.50	0.55
MYNN	-0.66	1.53	0.73	0.60	1.89	0.51	0.86	1.89	0.53	0.41	1.69	0.36	0.31	1.76	0.54
								RH/%							
YSU	-3.60	10.30	0.71	-2.11	11.15	0.73	-4.91	14.39	0.56	-10.78	17.49	0.56	-5.35	13.64	0.64
ACM2	-3.22	9.93	0.76	-3.82	11.69	0.72	-6.08	13.83	0.65	-12.63	19.08	0.53	-6.44	14.06	0.66
MYJ	-3.49	10.65	0.71	1.90	10.88	0.73	-4.35	14.67	0.51	-6.96	14.06	0.66	-3.22	12.74	0.65
MYNN	-4.44	10.01	0.75	-1.29	10.70	0.72	-4.36	13.70	0.60	-9.7	16.34	0.59	-4.05	12.70	0.67

412

413

414

415 Table 2 Statistics of WRF model performance with different PBL schemes in November, 2018

	Shanghai			Nanjing			Hangzhou			Hefei			Average		
	MB	RMSE	R	MB	RMSE	R	MB	RMSE	R	MB	RMSE	R	MB	RMSE	R
								T_2/℃							
YSU	0.83	1.80	0.85	0.68	2.12	0.87	1.23	2.13	0.85	0.83	2.07	0.89	0.89	2.03	0.88
ACM2	0.91	1.73	0.87	0.88	2.26	0.86	1.40	2.22	0.85	0.80	2.00	0.89	1.00	2.06	0.89
MYJ	0.84	1.70	0.87	0.67	2.10	0.87	1.22	2.08	0.86	0.68	2.12	0.87	0.85	2.01	0.89
MYNN	1.24	2.08	0.84	1.00	2.17	0.88	1.51	2.37	0.83	1.01	2.15	0.89	1.19	2.19	0.88
								WS_{10}/m·s^{-1}							
YSU	-0.31	1.35	0.60	0.60	1.35	0.66	0.33	1.23	0.49	0.56	1.41	0.55	0.28	1.34	0.56
ACM2	0.28	1.39	0.56	0.62	1.43	0.62	0.29	1.28	0.43	0.53	1.46	0.54	0.28	1.39	0.53
MYJ	-0.54	1.49	0.62	0.57	1.61	0.62	0.90	1.64	0.52	0.56	1.57	0.60	0.58	1.58	0.59
MYNN	-8.52	1.41	0.59	0.45	1.31	0.63	0.38	1.30	0.41	0.38	1.35	0.55	0.17	1.34	0.53
								RH/%							
YSU	-8.52	15.11	0.66	-6.21	14.82	0.67	-12.50	18.90	0.53	-6.78	13.03	0.80	-8.50	15.61	0.67
ACM2	-8.74	15.34	0.67	-8.26	15.85	0.66	-14.35	20.32	0.52	-8.81	14.67	0.78	-10.04	16.69	0.66
MYJ	-6.66	13.21	0.71	-3.23	13.06	0.68	-10.56	16.81	0.59	-3.01	11.85	0.78	-5.86	13.85	0.69
MYNN	-12.42	17.75	0.66	-8.12	14.25	0.74	-15.50	20.77	0.55	-8.09	12.87	0.84	-11.03	16.69	0.70

416

417

4 Conclusions

In this study, a seasonal sensitivity analysis study from the WRF mesoscale model is conducted to explore the impacts of four most commonly used PBL schemes (YSU, ACM2, MYJ and MYNN) on simulated meteorological variables over the YRD region in summer and winter. The WRF simulation indicates that the PBL schemes have different impact on meteorological variables in different seasons. Most the four PBL schemes underestimate the 2-m temperature in summer (-0.06~0.24℃ for July) while all the four PBL schemes overestimate the 2-m temperature in winter (0.17~0.52℃ for November). All the four PBL schemes overestimate 10-m wind speed (0.29~1.47m/s for July; 0.25~0.66m/s for November) and underestimate the relative humidity (-4.07~-5.86% for July; -5.86%~-11.03% for November). Warm bias in summer is mostly found in daytime, mainly as a consequence of overestimated breeze circulations. The warm deviation in winter is possibly related to the unresolved strong temperature inversion and the stability limitation of surface parameterisation. Wind speed of overestimation in summer is higher than winter. Diagnosis of the surface meteorological variables indicate that for temperature the local closure scheme MYNN simulated well in summer while MYJ performs better in winter. For wind speed, ACM2 scheme and the local closure scheme MYNN produced better simulations, and the MYJ and YSU schemes slightly overestimated the winds than the formers. For humidity, ACM2 and YSU schemes simulate reasonably well in summer and relatively underestimated in winter while the other three schemes produced close simulations and the MYNN performed larger bias in winter. Generally, the simulations of winter cases are better than that of summer cases, the reason is related to the relatively stable flow field in winter. MYNN performs better in meteorological factors than other three schemes in summer and MYJ provides better simulations in winter for the YRD region. Comparisons of the PBL heights reveal that except for the ACM2, other three PBL schemes show varying degrees of underestimation, with the MYJ scheme exhibits the largest underestimation and the MYNN scheme shows the smallest in summer. On the contrary, most PBL schemes especially the MYNN scheme produce the highest overestimation in winter. As for the diurnal cycle, the YSU and MYNN schemes exhibit more realistic time variation in the PBL heights in accordance with radiosonde data. All four schemes capture a strong diurnal PBL pattern of daily variation while the MYNN scheme performed the lowest MB and the ACM2 scheme provided the highest correlation coefficient in summer. While the MYJ scheme shows the best simulation with MB of -0.02km in winter.

In summary, we find that model systematic errors are dependent on the seasonal and daily cycles, and variable terrain conditions that causes different atmospheric factors. This is necessary to be

considered when selecting the most adequate model configuration or improving the parametrization schemes. Overall, the local PBL scheme MYNN performs well for model simulations of the meteorology and PBL height in summer while the local PBL scheme MYJ exhibits better simulation results in winter over the YRD region.

Acknowledgement

This study is financially supported by the National Natural Science Foundation of China (NO. 42075144, 41875161, 41105102), Shanghai International Science and Technology Cooperation Fund (NO. 19230742500), the National Key R&D Program of China (NO.2018YFC0213600), the Shanghai Science and Technology Innovation Plan (NO.19DZ1205007), and the Shanghai Sail Program (No. 19YF1415600). We thank Prof. Liu Cheng at University of Science and Technology of China for helping with derivation of the PBL data from Lidar measurement at Hefei, and thank Prof. Qingyan Fu at Shanghai Environmental Monitoring Center for providing the PBL data at Dianshan Lake station.

References

Ayotte, K. W., P. P. Sullivan, A. Andren, S. C. Doney, A. A. Holtslag, W. G. Large, J. C. McWilliams, C.-H. Moeng, M. J. Otte, and J. Tribbia (1996), An evaluation of neutral and convective planetary boundary-layer parameterizations relative to large eddy simulations, *Boundary-Layer Meteorology*, *79*(1-2), 131-175.

Banks, R. F., and J. M. Baldasano (2016), Impact of WRF model PBL schemes on air quality simulations over Catalonia, Spain, *Science of the total environment*, *572*, 98-113.

Bright, D. R., S. L. Mullen (2002), The sensitivity of the numerical simulation of the southwest monsoon boundary layer to the choice of PBL turbulence parameterization in MM5, *Weather and Forecasting*, *17*(1), 99-114.

Bryan, G. H., J. C. Wyngaard, and J. M. Fritsch (2003), Resolution requirements for the simulation of deep moist convection, *Monthly Weather Review*, *131*(10), 2394-2416.

Chaouch, N., M. Temimi, M. Weston, and H. Ghedira (2017), Sensitivity of the meteorological model WRF-ARW to planetary boundary layer schemes during fog conditions in a coastal arid region, *Atmospheric Research*, *187*, 106-127.

Chen, F., and J. Dudhia (2001), Coupling an advanced land surface–hydrology model with the Penn State–NCAR MM5 modeling system. Part I: Model implementation and sensitivity, *Monthly weather review*, *129*(4), 569-585.

Cheng, W. Y., W. J. Steenburgh, (2005), Evaluation of surface sensible weather forecasts by the WRF and the Eta models over the western United States, *Weather and Forecasting*, *20*(5), 812-821.

Chu, Y., J. Li, C. Li, W. Tan, T. Su, and J. Li (2019), Seasonal and diurnal variability of planetary boundary layer height in Beijing: Intercomparison between MPL and WRF results, *Atmospheric research*, *227*, 1-13.

Clark, A. J., M. C. Coniglio, B. E. Coffer, G. Thompson, M. Xue, F. Kong, (2015), Sensitivity of 24-h forecast dryline position and structure to boundary layer parameterizations in convection-allowing WRF

Model simulations, *Weather and Forecasting*, *30*(3), 613-638.
Cohen, A. E., S. M. Cavallo, M. C. Coniglio, H. E. Brooks, (2015), A review of planetary boundary layer parameterization schemes and their sensitivity in simulating southeastern US cold season severe weather environments, *Weather and forecasting*, *30*(3), 591-612.
Coniglio, M. C., J. Correia Jr, P. T. Marsh, F. Kong, (2013), Verification of convection-allowing WRF model forecasts of the planetary boundary layer using sounding observations, *Weather and Forecasting*, *28*(3), 842-862.
Cuchiara, G. C., X. Li, J. Carvalho, and B. Rappenglück (2014), Intercomparison of planetary boundary layer parameterization and its impacts on surface ozone concentration in the WRF/Chem model for a case study in Houston/Texas, *Atmospheric Environment*, *96*, 175-185.
Deppe, A. J., W. A. Gallus Jr, E. S. Takle, (2013), A WRF ensemble for improved wind speed forecasts at turbine height, *Weather and Forecasting*, *28*(1), 212-228.
Draxl, C., A. N. Hahmann, A. Peña, and G. Giebel (2014), Evaluating winds and vertical wind shear from Weather Research and Forecasting model forecasts using seven planetary boundary layer schemes, *Wind Energy*, *17*(1), 39-55.
García-Díez, M., J. Fernández, L. Fita, and C. Yagüe (2013), Seasonal dependence of WRF model biases and sensitivity to PBL schemes over Europe, *Quarterly Journal of the Royal Meteorological Society*, *139*(671), 501-514.
Garratt, J. R. (1994), The atmospheric boundary layer, *Earth-Science Reviews*, *37*(1-2), 89-134.
Giannaros, T. M., D. Melas, I. A. Daglis, I. Keramitsoglou, and K. Kourtidis (2013), Numerical study of the urban heat island over Athens (Greece) with the WRF model, *Atmospheric Environment*, *73*, 103-111.
Gopalakrishnan, S. G., F. Marks Jr, J. A. Zhang, X. Zhang, J.-W. Bao, and V. Tallapragada (2013), A study of the impacts of vertical diffusion on the structure and intensity of the tropical cyclones using the high-resolution HWRF system, *Journal of the atmospheric sciences*, *70*(2), 524-541.
Gunwani, P., and M. Mohan (2017), Sensitivity of WRF model estimates to various PBL parameterizations in different climatic zones over India, *Atmospheric Research*, *194*, 43-65.
Han, Z., H. Ueda, and J. An (2008), Evaluation and intercomparison of meteorological predictions by five MM5-PBL parameterizations in combination with three land-surface models, *Atmospheric Environment*, *42*(2), 233-249.
Hariprasad, K., C. V. Srinivas, A. B. Singh, S. V. B. Rao, R. Baskaran, and B. Venkatraman (2014), Numerical simulation and intercomparison of boundary layer structure with different PBL schemes in WRF using experimental observations at a tropical site, *Atmospheric Research*, *145*, 27-44.
Hogrefe, C., G. Pouliot, D. Wong, A. Torian, S. Roselle, J. Pleim, and R. Mathur (2015), Annual application and evaluation of the online coupled WRF–CMAQ system over North America under AQMEII phase 2, *Atmospheric Environment*, *115*, 683-694.
Holt, T., and S. Raman (1988), A review and comparative evaluation of multilevel boundary layer parameterizations for first-order and turbulent kinetic energy closure schemes, *Reviews of geophysics*, *26*(4), 761-780.
Hong, S.-Y., Y. Noh, and J. Dudhia (2006), A new vertical diffusion package with an explicit treatment of entrainment processes, *Monthly weather review*, *134*(9), 2318-2341.
Hong, S. Y. (2010), A new stable boundary-layer mixing scheme and its impact on the simulated East Asian summer monsoon, *Quarterly Journal of the Royal Meteorological Society*, *136*(651), 1481-1496.
Hu, X.-M., J. W. Nielsen-Gammon, F. Zhang, (2010), Evaluation of three planetary boundary layer schemes in the WRF model, *Journal of Applied Meteorology and Climatology*, *49*(9), 1831-1844.

Huang, M., Z. Gao, S. Miao, F. Chen, (2019), Sensitivity of urban boundary layer simulation to urban canopy models and PBL schemes in Beijing, *Meteorology and Atmospheric Physics*, *131*(5), 1235-1248.
Janjić, Z. I. (1990), The step-mountain coordinate: Physical package, *Monthly Weather Review*, *118*(7), 1429-1443.
Jia, W., and X. Zhang (2020), The role of the planetary boundary layer parameterization schemes on the meteorological and aerosol pollution simulations: A review, *Atmospheric Research*, *239*, 104890.
Jiménez, P. A., J. Dudhia, (2012), Improving the representation of resolved and unresolved topographic effects on surface wind in the WRF model, *Journal of Applied Meteorology and Climatology*, *51*(2), 300-316.
Kain, J. S., and J. M. Fritsch (1993), Convective parameterization for mesoscale models: The Kain-Fritsch scheme, in *The representation of cumulus convection in numerical models*, edited, pp. 165-170, Springer.
Kala, J., J. Andrys, T. J. Lyons, I. J. Foster, and B. J. Evans (2015), Sensitivity of WRF to driving data and physics options on a seasonal time-scale for the southwest of Western Australia, *Climate Dynamics*, *44*(3-4), 633-659.
Kwun, J. H., Y.-K. Kim, J.-W. Seo, J. H. Jeong, and S. H. You (2009), Sensitivity of MM5 and WRF mesoscale model predictions of surface winds in a typhoon to planetary boundary layer parameterizations, *Natural Hazards*, *51*(1), 63-77.
Lee, S.-m., W. Giori, M. Princevac, and H. Fernando (2006), Implementation of a stable PBL turbulence parameterization for the mesoscale model MM5: nocturnal flow in complex terrain, *Boundary-layer meteorology*, *119*(1), 109-134.
Li, L., An, J.Y., Zhou, M., Qiao, L.P., Zhu, S.H., Yan, R.S., Ooi, C. G., Wang, H.L., Lou, S. R., Huang, C., Tao, S.K., Chen, C.H., Yu, J.Z., Chan, A (2018), An integrated source apportionment methodology and its application over the Yangtze River Delta Region, China. *Environmental Science and Technology*. *52*(24), 14216-14227. DOI: 10.1021/acs.est.8b01211.
Li, L., Zhu, S. H., An, J.Y., Zhou, M., Wang, H.L., Yan, R. S., Qiao, L.P., Tian, X. D., Shen, L. J., Huang, L., Wang, Y. J., Huang, C., Avise, J. C., Fu, J. S.(2019), Evaluation of the effect of regional joint-control measures on changing photochemical transformation: a comprehensive study of the optimization scenario analysis. *Atmospheric Chemistry and Physics*. *19*, 9037-9060.
Li, L., An, J. Y., Yan, R. S., Huang, C., Wang, H. L., Lou, S. R., Huang, L., Yarwood, G (2019), Ozone source apportionment over the Yangtze River Delta region, China: Investigation of regional transport, sectoral contributions and seasonal differences. *Atmospheric Environment*, *2019, 202*: 269-280.
Li, P., G. Fu, C. Lu, D. Fu, S. Wang, (2012), The formation mechanism of a spring sea fog event over the Yellow Sea associated with a low-level jet, *Weather and Forecasting*, *27*(6), 1538-1553.
Li, T., H. Wang, T. Zhao, M. Xue, Y. Wang, H. Che, and C. Jiang (2016), The impacts of different PBL schemes on the simulation of PM2. 5 during severe haze episodes in the Jing-Jin-Ji region and its surroundings in China, *Advances in Meteorology*, *2016*.
Li, Y., Yin, S., Yu, S., Bai, L., Wang, X., Lu, X., Ma, S (2021). Characteristics of ozone pollution and the sensitivity to precursors during early summer in central plain, China. *Journal of Environmental Sciences*, *99*, 354-368.
Lin, Y.-L., R. D. Farley, H. D. Orville, (1983), Bulk parameterization of the snow field in a cloud model, *Journal of Climate Applied Meteorology*, *22*(6), 1065-1092.
Lo, J. C. F., Z. L. Yang, and R. A. Pielke Sr (2008), Assessment of three dynamical climate downscaling methods using the Weather Research and Forecasting (WRF) model, *Journal of Geophysical Research:*

578 *Atmospheres*, *113*(D9).
579 Madala, S., A. Satyanarayana, C. Srinivas, and M. Kumar (2015), Mesoscale atmospheric flow-field
580 simulations for air quality modeling over complex terrain region of Ranchi in eastern India using WRF,
581 *Atmospheric Environment*, *107*, 315-328.
582 Mallard, M. S., C. G. Nolte, O. R. Bullock, T. L. Spero, and J. Gula (2014), Using a coupled lake model
583 with WRF for dynamical downscaling, *Journal of Geophysical Research: Atmospheres*, *119*(12), 7193-
584 7208.
585 Misenis, C., and Y. Zhang (2010), An examination of sensitivity of WRF/Chem predictions to physical
586 parameterizations, horizontal grid spacing, and nesting options, *Atmospheric Research*, *97*(3), 315-334.
587 Mlawer, E. J., S. J. Taubman, P. D. Brown, M. J. Iacono, and S. A. Clough (1997), Radiative transfer for
588 inhomogeneous atmospheres: RRTM, a validated correlated-k model for the longwave, *Journal of*
589 *Geophysical Research: Atmospheres*, *102*(D14), 16663-16682.
590 Moeng, C.-H. J. J. o. t. A. S. (1984), A large-eddy-simulation model for the study of planetary boundary-
591 layer turbulence, *Journal of the Atmospheric Sciences*, *41*(13), 2052-2062.
592 Mohan, M., and S. J. A. i. M. Bhati (2011), Analysis of WRF model performance over subtropical region
593 of Delhi, India, *Advances in Meteorology*, *2011*.
594 Mölders, N. (2008), Suitability of the Weather Research and Forecasting (WRF) model to predict the
595 June 2005 fire weather for Interior Alaska, *Weather and Forecasting*, *23*(5), 953-973.
596 Mughal, M. O., X. X. Li, T. Yin, A. Martilli, O. Brousse, M. A. Dissegna, and L. K. Norford (2019),
597 High-Resolution, Multilayer Modeling of Singapore's Urban Climate Incorporating Local Climate Zones,
598 *Journal of Geophysical Research: Atmospheres*, *124*(14), 7764-7785.
599 Nakanishi, M., and H. Niino (2006), An improved Mellor–Yamada level-3 model: Its numerical stability
600 and application to a regional prediction of advection fog, *Boundary-Layer Meteorology*, *119*(2), 397-407.
601 Ni, Z. Z., Luo, K., Zhang, J. X., Feng, R., Zheng, H. X., Zhu, H. R., Cen, K. F (2018). Assessment of
602 winter air pollution episodes using long-range transport modeling in Hangzhou, China, during World
603 Internet Conference, 2015, *Environmental pollution*, *236*, 550-561.
604 Ooi, M.C.G, Chan, A., Subramaniam, K., Morris, K.I. & Oozeerm, M.Y. (2018), Interactions of Urban
605 Heating and Local Winds During the Calm Intermonsoon Seasons in the Tropics, *Journal of Geophysical*
606 *Research: Atmospheres*, *122*(11), 11499-11523.
607 Oozeer, M.Y. Chan, A., Ooi, M.C.G., Zarzur, A..M., Salinas, S.V., Chew, B.N., Morris, K.I., & Choong,
608 W.K (2016), Numerical study of the transport and convective mechanisms of biomass burning haze in
609 South-Southeast Asia, *Aerosol and Air Quality Research*, 16, 2950-2963
610 Penchah, M. M., H. Malakooti, and M. Satkin (2017), Evaluation of planetary boundary layer simulations
611 for wind resource study in east of Iran, *Renewable Energy*, *111*, 1-10.
612 Pleim, J. E. (2007), A combined local and nonlocal closure model for the atmospheric boundary layer.
613 Part I: Model description and testing, *Journal of Applied Meteorology and Climatology*, *46*(9), 1383-
614 1395.
615 Román-Cascón, C., C. Yagüe, M. Sastre, G. Maqueda, F. Salamanca, S. Viana (2012), Observations and
616 WRF simulations of fog events at the Spanish Northern Plateau, *Advances in Science and Research*, *8*(1),
617 11-18.
618 Sanjay, J. (2008), Assessment of atmospheric boundary-layer processes represented in the numerical
619 model MM5 for a clear sky day using LASPEX observations, *Boundary-layer meteorology*, *129*(1), 159-
620 177.
621 Shen, L., Zhao, C., Ma, Z., Li, Z., Li, J., Wang, K (2019). Observed decrease of summer sea-land breeze

in Shanghai from 1994 to 2014 and its association with urbanization, *Atmospheric Research*, *227*, 198-209.

Shin, H. H., and S.-Y. Hong (2011), Intercomparison of planetary boundary-layer parametrizations in the WRF model for a single day from CASES-99, *Boundary-Layer Meteorology*, *139*(2), 261-281.

Skamarock, W. C., J. B. Klemp, J. Dudhia, D. O. Gill, D. M. Barker, M. G. Duda, X.-Y. Huang, W. Wang, and J. G. Powers (2008), G.: A description of the Advanced Research WRF version 3, paper presented at NCAR Tech. Note NCAR/TN-475+ STR, Citeseer.

Smith, R. K., and G. L. Thomsen (2010), Dependence of tropical-cyclone intensification on the boundary-layer representation in a numerical model, *Quarterly Journal of the Royal Meteorological Society*, *136*(652), 1671-1685.

Steele, C., S. Dorling, R. Von Glasow, J. Bacon (2013), Idealized WRF model sensitivity simulations of sea breeze types and their effects on offshore windfields, *Atmospheric Chemistry and Physics*, *13*(1), 443.

Su, L., and J. C. Fung (2015), Sensitivities of WRF-Chem to dust emission schemes and land surface properties in simulating dust cycles during springtime over East Asia, *Journal of Geophysical Research: Atmospheres*, *120*(21), 11,215-211,230.

Sullivan, P. P., J. C. McWilliams, and C.-H. Moeng (1994), A subgrid-scale model for large-eddy simulation of planetary boundary-layer flows, *Boundary-Layer Meteorology*, *71*(3), 247-276.

Wang, C. g., L. Feng, C. Le, Y. Jiade, and J. Hai-Mei (2017a), Comparison and analysis of several planetary boundary layer schemes in WRF model between clear and overcast days, *Chinese Journal of Geophysics*, *60*(2), 141-153.

Wang, Y., S. Di Sabatino, A. Martilli, Y. Li, M. Wong, E. Gutiérrez, and P. Chan (2017b), Impact of land surface heterogeneity on urban heat island circulation and sea-land breeze circulation in Hong Kong, *Journal of Geophysical Research: Atmospheres*, *122*(8), 4332-4352.

Wang, Z., A. Duan, and G. Wu (2014), Impacts of boundary layer parameterization schemes and air-sea coupling on WRF simulation of the East Asian summer monsoon, *Science China Earth Sciences*, *57*(7), 1480-1493.

Xie, B., J. C. Fung, A. Chan, and A. Lau (2012), Evaluation of nonlocal and local planetary boundary layer schemes in the WRF model, *Journal of Geophysical Research: Atmospheres*, *117*(D12).

Yerramilli, A., V. S. Challa, V. B. R. Dodla, H. P. Dasari, J. H. Young, C. Patrick, J. M. Baham, R. L. Hughes, M. G. Hardy, and S. J. Swanier (2010), Simulation of surface ozone pollution in the central gulf coast region using WRF/Chem Model: Sensitivity to PBL and Land Surface Physics, *Advances in Meteorology*, *2010*.

Yver, C., H. Graven, D. D. Lucas, P. Cameron-Smith, R. Keeling, R. Weiss (2013), Evaluating transport in the WRF model along the California coast, *Atmospheric Chemistry & Physics*, *13*(4).

Zhang, D.-L., and W.-Z. J. Zheng (2004), Diurnal cycles of surface winds and temperatures as simulated by five boundary layer parameterizations, *Journal of Applied Meteorology and Climatology*, *43*(1), 157-169.

Zhang, Q., Zhang, J., Qiao, J., & Wang, S (2011), Relationship of atmospheric boundary layer depth with thermodynamic processes at the land surface in arid regions of China, *Science China Earth Sciences*, *54*(10), 1586.

Supplement of

The impact of planetary boundary layer parameterisation over the Yangtze River Delta region, China - Part I: meteorological simulation

Ansheng Zhu [a,b], Lishu Shi [a,b], Ling Huang [a,b], Ying Gu [c], Yangjun Wang [a,b], Andy Chan [d], Li Li [a,b*]*

[a] School of Environmental and Chemical Engineering, Shanghai University, Shanghai 200444, China

[b] Key Laboratory of Organic Compound Pollution Control Engineering (MOE), Shanghai University, Shanghai 200444, China

[c] School of air transportation, Shanghai University of Engineering Science, Shanghai 201620, China

[d] Department of Civil Engineering, University of Nottingham Malaysia, Semenyih 43500, Selangor, Malaysia

Correspondence to Li Li (Lily@shu.edu.cn) and Andy Chan (Andy.Chan@nottingham.edu.my)

Fig S1. Spatial distribution of 2-m temperature simulated with the WRF model using each of the four PBL schemes during July and November.

Fig. S2. Spatial distribution of 10-m wind speed simulated with the WRF model using each of the four PBL schemes during July and November.

Fig. S3. Spatial distribution of relative humidity simulated with the WRF model using each of the four PBL schemes during July and November.

Fig. S4. Spatial distribution of PBL height simulated with the WRF model using each of the four PBL schemes during July and November.

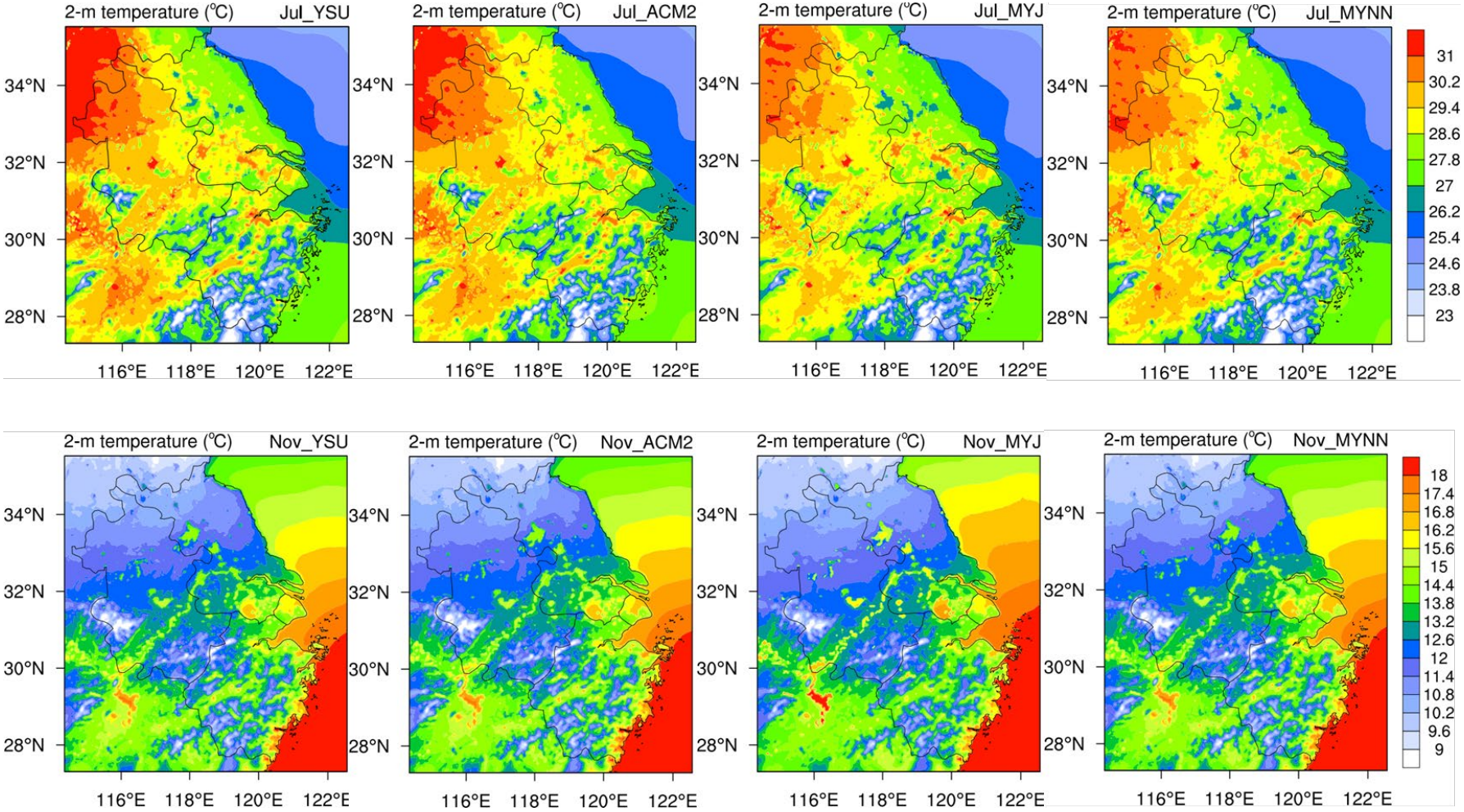

Fig. S1. Spatial distribution of 2-m temperature simulated with the WRF model using each of the four PBL schemes during July and November.

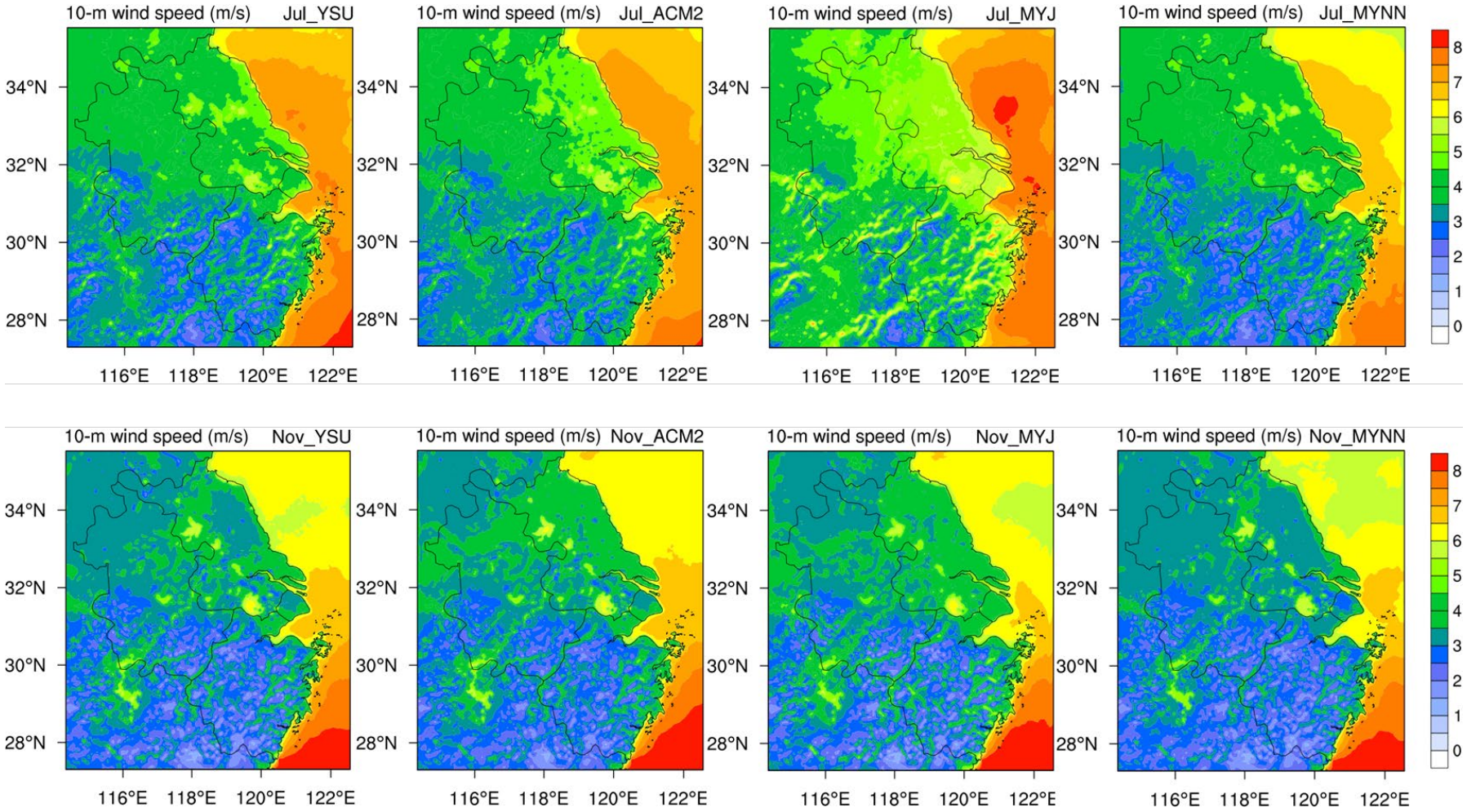

Fig. S2. Spatial distribution of 10-m wind speed simulated with the WRF model using each of the four PBL schemes during July and November.

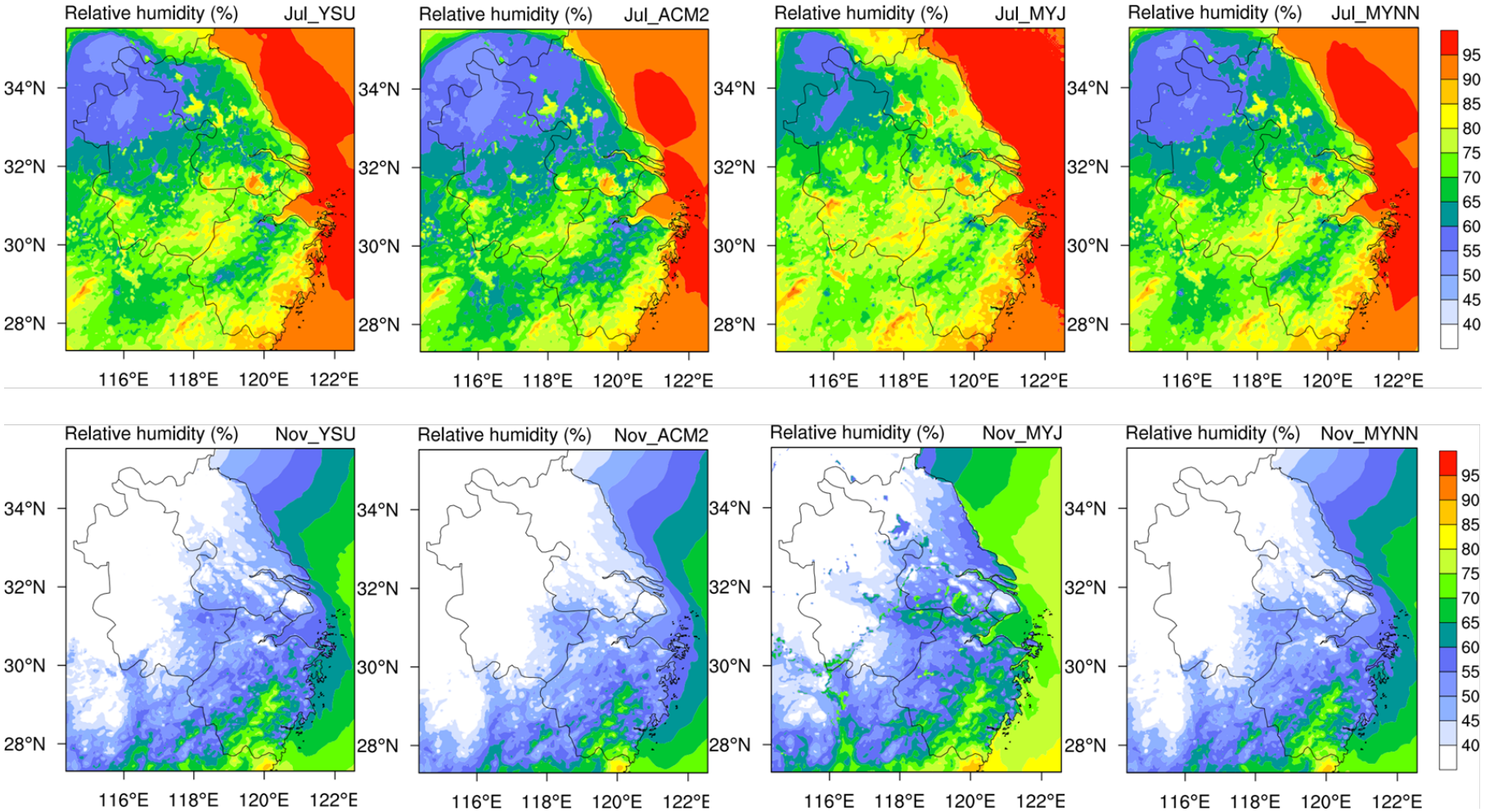

Fig. S3. Spatial distribution of relative humidity simulated with the WRF model using each of the four PBL schemes during July and November.

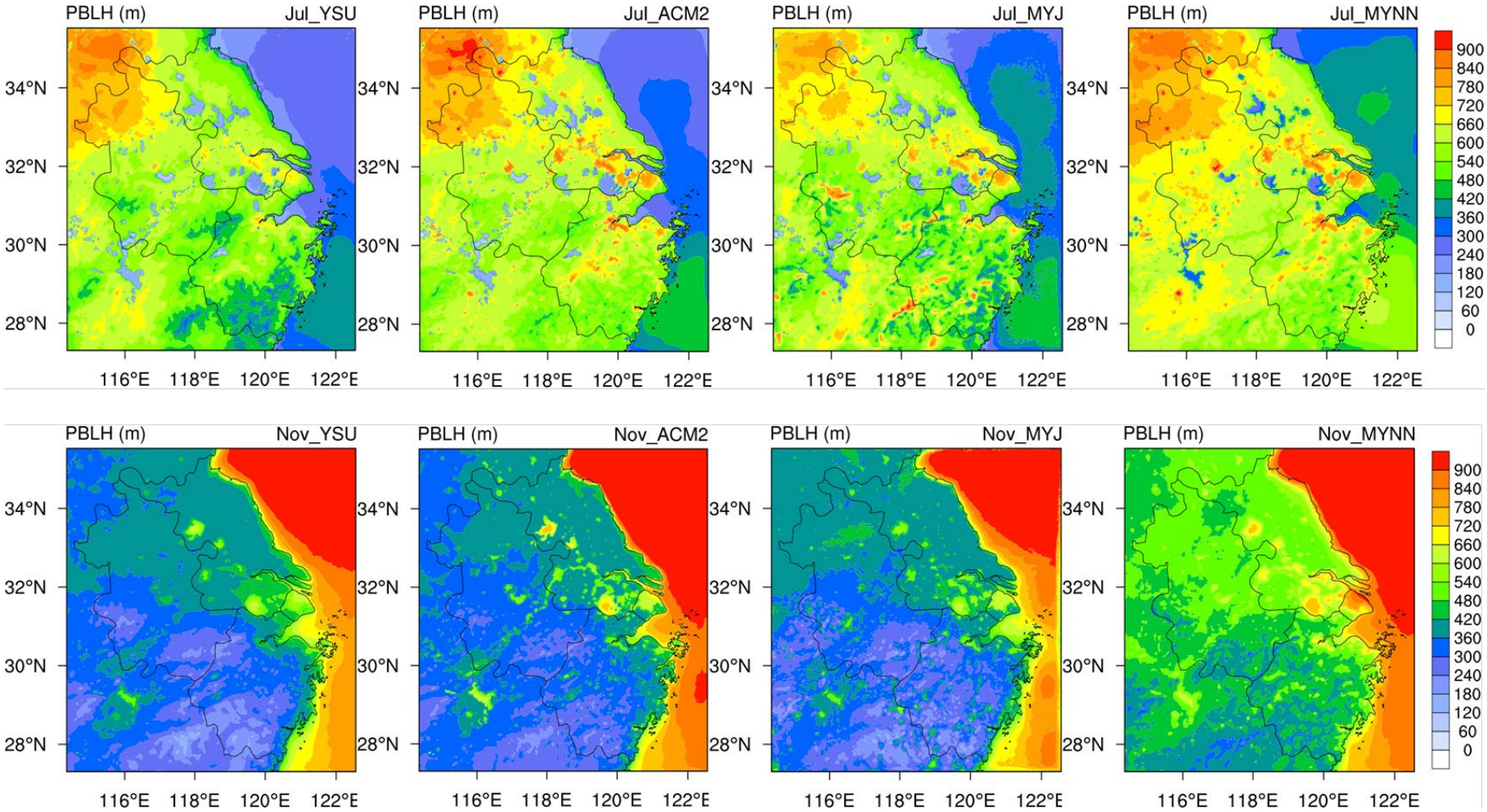

Fig. S4. Spatial distribution of PBL height simulated with the WRF model using each of the four PBL schemes during July and November.